



**HAL**  
open science

# Numerical modelling of heat and mass transfer in finned dehumidifier

Giulio Croce, Erika de Candido, Paola d'Agaro

## ► To cite this version:

Giulio Croce, Erika de Candido, Paola d'Agaro. Numerical modelling of heat and mass transfer in finned dehumidifier. *Applied Thermal Engineering*, 2009, 29 (7), pp.1366. 10.1016/j.applthermaleng.2008.05.003 . hal-00595945

**HAL Id: hal-00595945**

**<https://hal.science/hal-00595945>**

Submitted on 26 May 2011

**HAL** is a multi-disciplinary open access archive for the deposit and dissemination of scientific research documents, whether they are published or not. The documents may come from teaching and research institutions in France or abroad, or from public or private research centers.

L'archive ouverte pluridisciplinaire **HAL**, est destinée au dépôt et à la diffusion de documents scientifiques de niveau recherche, publiés ou non, émanant des établissements d'enseignement et de recherche français ou étrangers, des laboratoires publics ou privés.

## Accepted Manuscript

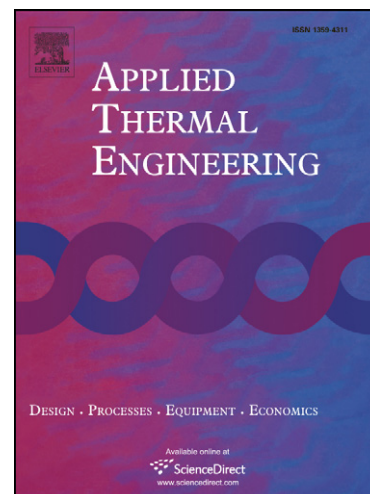
Numerical modelling of heat and mass transfer in finned dehumidifier

Giulio Croce, Erika De Candido, Paola D'Agaro

PII: S1359-4311(08)00220-2  
DOI: [10.1016/j.applthermaleng.2008.05.003](https://doi.org/10.1016/j.applthermaleng.2008.05.003)  
Reference: ATE 2506

To appear in: *Applied Thermal Engineering*

Received Date: 11 December 2007  
Revised Date: 2 May 2008  
Accepted Date: 6 May 2008



Please cite this article as: G. Croce, E. De Candido, P. D'Agaro, Numerical modelling of heat and mass transfer in finned dehumidifier, *Applied Thermal Engineering* (2008), doi: [10.1016/j.applthermaleng.2008.05.003](https://doi.org/10.1016/j.applthermaleng.2008.05.003)

This is a PDF file of an unedited manuscript that has been accepted for publication. As a service to our customers we are providing this early version of the manuscript. The manuscript will undergo copyediting, typesetting, and review of the resulting proof before it is published in its final form. Please note that during the production process errors may be discovered which could affect the content, and all legal disclaimers that apply to the journal pertain.

Submitted for publication in  
APPLIED THERMAL ENGINEERING  
Special Issue: 10<sup>th</sup> UK Heat Transfer

**Numerical modelling of heat and mass transfer in finned dehumidifier**

**Giulio Croce\*, Erika De Candido, Paola D'Agaro**

DiEM, Dipartimento di Energetica e Macchine

Università di Udine,

Via delle Scienze 208, 33100

ITALY

\*Corresponding author:

tel: +39 432 558018; fax: +39 432 558027; e-mail: giulio.croce@uniud.it

Short title: Heat and mass transfer in dehumidifier

*Abstract:* - In several heat exchange devices phase transition occurs in a small region adjacent to the wall, and the secondary phase is present only in a thin layer running along the wall, allowing for decoupling between the fluid dynamic computation of the core flow and the numerical analysis of the secondary phase. This happens in finned dehumidifier, but also in spray cooling or defogging problems. In a finned dehumidifier, or in air conditioning evaporators, the secondary phase is provided by moist air condensation, and may consist of discrete droplets, continuous film or a collection of rivulets. Several levels of approximation may be adopted, depending on the specific problem: perfect drain assumption requires only the addition of a heat source in the energy equation, otherwise the water layer behaviour has to be taken into account. Furthermore, an heat and mass transfer analogy may or may not be appropriate; in the latter case, the solution of the diffusion equation of humidity is required.

Here, different levels of approximation are compared with literature experimental data for condensation over a vertical fin. Results show that thermal resistance and gravity effects, in the considered geometry, are negligible, and the condensate takes the form of a collection of still droplets, rather than a flowing film. This has an effect on the actual heat transfer and water layer build-up, and the variation of temperature along the fin induces some discrepancy with respect to the straightforward application of the heat and mass transfer analogy.

*Key-Words:* - finned dehumidifier, condensation, droplet, film, moist, mass transfer

## 1 Nomenclature

$A_{dry}$	dry solid area, eq.(16), $m^2$
$A_{wet}$	droplet/solid contact area, eq.(16), $m^2$
$A_{cap}$	droplet/air contact area, eq.(16), $m^2$
$A_t$	total area of an interface element, $m^2$
$Bo$	Bond number, dimensionless, $Bo = \rho g d^2 \sin \alpha / \sigma$
$c$ ,	solid specific heat $J/(kg K)$
$c_p$	air constant pressure specific heat, $J/(kg K)$
$D$	diffusion coefficient, $m^2/s$
$d$	droplet base diameter, $m$
$g$	acceleration of gravity, $m/s^2$
$h$	heat transfer coefficient, $W/(m^2K)$
$h_w$	water layer cell-averaged height, $m$
$H$	fin vertical length, $m$
$k$	thermal conductivity, $W/(m K)$
$L$	fin streamwise extension, $m$
$\dot{m}''$	water mass flow rate per unit surface $kg/(m^2s)$
$\dot{m}'$	water mass flow per unit length, $kg/(m s)$
$M$	molecular weight, $kg/kmol$
$n$	unit vector normal to the boundary
$p$	Pressure, $Pa$
$Pr$	Prandtl number, dimensionless, $Pr = \mu_f c_p / k_f$
$Q''$	heat flux per unit surface, $W/m^2$
$R_v$	air gas constant, $J/(kg K)$
$Sc$	Schmidt number, dimensionless, $Sc = \mu_f / \rho_f D$
$T$	Absolute temperature, $K$
$v$	fluid velocity, $m/s$
$x, y, z$	Cartesian coordinates, $m$
<i>Greek symbols</i>	
$\alpha$	surface inclination angle, $rad$
$\phi$	relative humidity, dimensionless
$\Gamma$	solid/fluid interface
$\lambda$	latent heat of evaporation, $J/kg$
$\mu$	dynamic viscosity, $kg/(m s)$
$\vartheta$	time, $s$
$\theta$	water/solid contact angle, $rad$
$\rho$	density, $kg/m^3$
$\sigma$	surface tension of the liquid/vapor interface, $N/m$
$\tau$	wall shear stress, $N/m^2$
$\omega$	mass fraction of water vapor, $kg_{vapor}/kg_{moist air}$
$\psi$	droplet azimuthal angle, $rad$
<i>Subscripts and superscripts</i>	
$0$	freestream

<i>adv</i>	advancing
<i>conv</i>	convective
<i>f</i>	fluid
<i>lat</i>	latent
<i>min</i>	minimum value
<i>n</i>	current time step
<i>rec</i>	receding
<i>s</i>	solid
<i>sat</i>	saturation
<i>v</i>	water vapor
<i>w</i>	water layer

ACCEPTED MANUSCRIPT

## 1 Introduction

Gas-liquid phase transition often occurs in a small region adjacent to solid walls, and the secondary phase is present only in a thin layer running along the wall. This happens in several heat transfer devices, including finned condensers or finned dehumidifier [1-3], but also in spray cooling [4] or fogging/defogging problems [5]. In such situation, we have three different domains (air flow domain, water flow region, solid), possibly governed by three different set of equations (compressible/incompressible flow, conduction problem, shallow water models). The interaction among these domains can be modelled with different levels of detail, depending on the flow and thermal conditions.

It is common practice, for example, to decouple the fluid dynamic computation of the core flow and the numerical analysis of the secondary, liquid, phase. In the core flow the solution of continuity, momentum, energy and mass diffusion equation are required. However, the mass diffusion equation is sometimes skipped, relying on the well known heat and mass transfer analogy to obtain mass transfer data from the energy equation. Unfortunately, the heat and mass transfer analogy holds true under some constraints: as an example, we obviously need to have analogy both in the equation, which is easily verified, and in the boundary conditions. The latter is not always true: in a partially wet fin the mass diffusion equation requires Neumann conditions (no mass flow) in the dry areas, and Dirichlet boundary conditions (concentration equal to saturation threshold) in the wet regions, while the energy equation will more likely have either Neumann or Dirichlet boundaries on the whole surface. Furthermore, analogy is well respected in a boundary-layer like flow regime, but can easily fail in more complex flow regimes [6].

In a finned dehumidifier, or in a finned air conditioning evaporator, the secondary phase is the liquid layer produced by moist air condensation, and may consist of discrete droplets, as in fogging phenomena, continuous film or a collection of rivulets. Again, several levels of modelling approximation may be adopted, depending on the specific problem: if perfect drainage is assumed, the condensing effect can be effectively described by a simple heat source in the energy equation [7], otherwise the film development has to be taken into account.

The full description of the fluid-dynamic behaviour of the water layer is a very complex task which involves the numerical solution of the flow field both inside and outside the liquid film/droplet, thus requiring specific computational techniques for the simulation of moving boundaries at the interface [8, 9]. This is particularly challenging in the case of dropwise condensation, which in principle would require the simulation of each droplet. Such a level of detail is not viable for simultaneous solution on thermal and flow field in complex geometries; furthermore, it might not be necessary when the aim is the evaluation of the condensation effect on the global heat transfer device performances.

In the present paper we take into account the details of the water layer status for those aspects which may have direct impact on the actual latent heat transfer rate, namely its configuration (collection of still droplet or moving film), driven by surface tension effect [3]. In particular, we are looking for more realistic interfacial boundary conditions obtained from the computation of some relevant parameters (dry/wet area ratio, face average water layer thermal resistance and obstruction) influencing the heat exchange.

We implemented a water layer model which is based on the experimental results by Korte et al. [10], ElSherbini et al. [11] Hu et al. [12], who, among others, discussed the possible influence of droplets and film configurations. As reported in literature, moist air

begins condensation at random location in the form of tiny beads. Surface tension forces at first inhibit the displacement of such tiny droplets. As their number increases, adjacent droplets start to coalesce. The base area of the larger droplet resulting from the coalescence of two smaller ones is smaller than the sum of the parent droplets. Thus, new portion of dry surface may be generated. This quickly leads to a self-similar condition [13,14], in which, although the average droplet size increases, the ratio between dry and wet area is constant, as well as the ratio between the total, curved, droplet surface area and the base one. These area ratios have an impact on heat transfer rate, since, as an example, we will have a mix of simple convective/conduction heat transfer through the dry portions, and condensation on the curved upper surface of the droplets [5]. Thus, neglecting droplet deformation, self similar configuration of still water droplets corresponds to a stable regime in heat transfer mechanisms, at least until the droplets become large enough for the gravity and shear stress forces to overcome the surface tension and start the water motion. This will lead to a different flow and heat transfer regime, either of continuous film, moving droplets or rivulets, depending on the water volume and flow conditions.

The main aim of this paper is to evaluate the different modelling options in the framework of an integrated CFD simulation, in the case of a vertical finned dehumidifier, under laminar flow conditions. In particular, the water layer regime (still droplets or continuous film) is detected taking into account the effects of gravity, shear stress and surface tension. Water thermal resistance, as well as the effect of film obstruction are also modelled. However, under the assumed range of flow and temperature conditions, the results show that the effects of the thermal resistance and the film obstructions were negligible, while the water layer assume the form of still droplets for a long time. Thus, the investigation is focused on the differences in the results obtained by a standard continuous

film and a droplet collection water layer model, and on the limits of applicability of the heat and mass transfer analogy, with special regard to the mixed dry-wet fin conditions.

All of the computations are carried out using an in-house finite element code for the solution of the air flow domain [16], a finite volume code for the solid solution, and a interfacial procedure for the conjugate heat transfer coupling which include the solution of the water layer governing equations [5].

## 2 Physical problem and computational domain

As a sample problem, the vertical fin array analyzed by Lin et al.[1] has been considered. The geometry, shown in Fig.1a, is made by an array of vertical, two millimeter thick, aluminium alloy fins. The spacing between adjacent fins is 3 mm and the fin area is  $L \times H = 100 \times 100$  mm. The range of air velocities (0.3-1.5 m/s) lies within the laminar regime. Inlet air flow is characterized by an inlet temperature of 300 K, and the inlet relative humidity  $\phi$  (ratio between actual partial vapour pressure and saturation pressure) ranges from 50% to 90%. Moist can condensate on the fin surface, as the base fin temperature is kept constant at 282 K, i.e. below dew point temperature. In the experimental set up, fin temperature is recorded by two series of thermocouples placed within the fins, along vertical lines at 25 and 75 mm from the fin channel inlet, i.e.  $\frac{1}{4}$  and  $\frac{3}{4}$  of the fin total streamwise extension  $L$ .

Due to symmetry conditions, the computational domain is reduced to one half of a single fin channel, spanning from the midplane of a fin to the midplane of the corresponding flow channel. Symmetry boundary conditions apply to both vertical planes, and a fixed temperature of 282 K is imposed on the base plane of the domain. No slip condition is enforced on all the solid walls, and constant Dirichlet boundary conditions for

the velocities, temperature and humidity are assumed at the inlet section. The fin top plane is assumed adiabatic.

### 3 Numerical Method

The physical problem involves a solid domain (the fin), a fluid domain for the air flow, and the water layer domain (Fig. 1b). The effect of atmospheric moist on thermophysical air properties is usually negligible. Thus, the air flow domain is governed by the continuity, momentum and energy equations for an incompressible, constant properties fluid:

$$\nabla \cdot \mathbf{v} = 0$$

$$\rho_f \frac{\partial \mathbf{v}}{\partial \vartheta} + \rho_f \mathbf{v} \cdot \nabla \mathbf{v} = \mu_f \nabla^2 \mathbf{v} - \nabla p \quad (1)$$

$$\rho_f c_p \frac{\partial T}{\partial \vartheta} + \rho_f c_p \mathbf{v} \cdot \nabla T = k_f \nabla^2 T$$

Two modelling options are compared for the evaluation of the condensing flow rate: the heat and mass transfer analogy vs the full simulation of the humidity transport. In the latter case, the mass diffusion equation is written in terms of the mass fraction of water vapour in moist air  $\omega$ :

$$\frac{\partial \omega}{\partial \vartheta} + \mathbf{v} \cdot \nabla \omega = D \nabla^2 \omega. \quad (2)$$

The solid domain requires the solution of the conduction equation

$$\rho_s c \frac{\partial T}{\partial \vartheta} = k_s \nabla^2 T. \quad (3)$$

As long as perfect drainage is assumed, the interaction between mass diffusion and energy equations can be modelled as a simple heat source [7]. In order to analyze the

detail of the water behaviour, some more detailed approaches can be followed. Here, a procedure derived from one previously adopted for icing and demisting problems [4] is adopted. The fluid and solid domains are solved independently, possibly with different codes. The interaction between these domains is handled by an interfacial procedure which takes into proper account the water layer.

Here, the flow field continuity, momentum and energy equations (Eq.(1)) are solved by an in-house finite element code [16], which allows for the solution of the mass transfer equation (2) as well [6,7]. The solid domain conduction problem (Eq.(3)) is computed by an efficient, structured finite volume code well suited for these simple geometries.

The computational grids for both the fluid and solid domains (Fig.1b) present 40 nodes in the x direction (flow), 80 nodes in y direction, 10 and 20 nodes in the z direction respectively.

The coupling of the two domains is here obtained via an exchange of boundary conditions. In the present simple geometry the fluid and solid grids have been built to match at the interface, thus the correspondence of element faces and nodes ensures the accuracy in the exchange of boundary conditions. In general the procedure presents maximum flexibility, since not only the two solvers of the solid and the fluid domain may be different, but non-matching grids might also be used. In the latter case the accuracy in the is handled by an ad hoc conservative interpolation procedure is closely similar to the one described in [18].

The coupling procedure can be summarized as in the following:

1. Continuity, Navier Stokes and energy equation Eq. (1) are solved for the fluid domain with the previous time step fluid temperature as a boundary condition  $T = T_f^n$  at fluid/solid interface  $\Gamma$

$$T = T_f^n \quad \text{on } \Gamma \quad (4)$$

2. The interface mass transfer is evaluated either via the solution of its transport equation eq.(2), assuming the appropriate boundary condition, or estimated from the heat transfer rate via the heat and mass transfer analogy.
3. The interfacial program evaluates the water layer thickness  $h_w$ , choosing between continuous film and still droplets regime. Furthermore, it computes the total heat flux, sum of the convective heat flux and the latent heat flux, to be given to the solid solver as the boundary condition for the conduction equation.
4. The conduction equation Eq.(3) is solved in the solid domain with the Neumann boundary condition at the fluid/solid interface,

$$\frac{\partial T}{\partial n} = -\frac{Q_s''}{k_s} \quad \text{on } \Gamma \quad (5)$$

yielding a new estimate of solid wall temperature  $T_s^{n+1}$  on the interface  $\Gamma$ :

5. Fluid flow boundary condition is estimated from the wall temperature taking into account the film thermal resistance. If  $k_w$  is the water thermal conductivity:

$$T_f^{n+1} = T_s^{n+1} + \frac{h_w}{k_w} Q_s'' \quad \text{on } \Gamma \quad (6)$$

6. Repeat from step 1.

At step 2. the proper mass transfer boundary conditions are required. In the wet region of the fin, the water mass fraction is equal to the saturation value, and thus a Dirichlet boundary condition is imposed

$$\omega = \omega_{sat}(T) = \frac{p_{sat}(T)}{\rho_f R_v T} \quad (7)$$

where the saturation pressure  $p_{sat}$  is given as

$$p_{sat}(T) = 610.78e^{\left(\frac{17.2694(T-273.15)}{T+34.85}\right)} \quad (8)$$

and  $T$  and  $p$  are given in K and Pa, respectively.

In the dry region a zero Neumann condition is required

$$\frac{\partial \omega}{\partial n} = 0. \quad (9)$$

### 3.1 Water layer modeling

For the analysis of the water layer a two dimensional finite volume grid is defined on the solid-fluid interface. In the present simple geometry such grid coincides with the fluid (or solid) grid on the interface. Proper water layer integral energy and mass balance for each element of this grid are needed in order to provide the proper boundary conditions for both solid and fluid domains.

Neglecting the water layer thermal capacity, as reasonable for thin layers, the energy balance of the condensate requires that the heat flux to the solid compensate the sum of the convective heat flux from the fluid and the latent heat contribution from condensation:

$$Q_s'' = Q_{conv}'' + Q_{lat}'' \quad (10)$$

where  $Q_s''$  is the total conduction heat flux per unit of area transferred to the solid,  $Q_{conv}''$  is the convective heat flux per unit of area from air, and  $Q_{lat}''$  is the latent heat flux per unit of area released in condensation process. During evaporation, the same equation holds true, but the latent heat contribution is negative. If  $\dot{m}_c''$  is the condensing water

mass flow and  $\lambda(T_f)$  the latent heat of vaporization at the water layer surface temperature, the latent heat contribution is given by

$$Q''_{lat} = \dot{m}''_c \lambda(T_f) \quad (11)$$

The value of condensing mass flow can be computed either via the proper diffusion equation (Eq.(2)) solution, adopting a consistent finite element approach following Comini et al., or estimated via an heat and mass transfer analogy. In this case, the condensing mass flow is a function of the local heat transfer coefficient  $h$ :

$$\dot{m}''_c = \frac{h}{c_p} \left( \frac{\text{Pr}}{\text{Sc}} \right)^{\frac{2}{3}} \frac{M_w}{M_f} \left( \frac{p_{sat_w} - \phi_0 p_{sat_0}}{p_0 - p_{sat_w}} \right) \quad (12)$$

where Pr is the Prandtl number of air, Sc is the Schmidt number for air,  $p_{sat_w}$  is the saturated steam pressure at the water layer temperature,  $p_{sat_0}$  is the saturated steam pressure at free stream temperature,  $p_0$  is the free stream pressure and  $\phi_0$  is the free stream humidity.

### 3.2 Film condensation

Under the assumption of continuous moving film the continuity equation must be solved in the 2D water layer domain. Since we are not solving the complete fluid dynamic equations within the water layer, we need some more hypothesis: for a thin film, we can assume a linear distribution of velocity through the film, as in a Couette flow. Under this assumption the shear stress is constant through the film and, thus, is possible to compute the runback water mass flow per unit length as:

$$\dot{m}'_{rb} = \frac{1}{2} \rho_w \frac{\tau}{\mu} h_w^2 \quad (13)$$

where  $\tau$  is the resulting stress from the fluid solution, and  $h_w$  is the local film height. If the gravity force  $\rho_w g h_w$  is effective, the film driving force is the resulting of gravity and shear stress, rather than the simple  $\tau$ . The balance of a generic 2D element  $\Omega$  on the interface, with a boundary  $\partial\Omega$ , becomes:

$$\int_{\partial\Omega} \dot{m}'_{rb} + \int_{\Omega} \dot{m}''_c = 0 \quad (14)$$

which is discretized with a first order upwind scheme. Since the shear stress  $\tau$  is known from the flow solution, the discretized form of Eq.(14) can be solved for the film height  $h_w$  via eq.(13).

Once  $h_w$  is known, it is possible to compute the slip velocity for the flow, i.e. the film velocity at the air-water interface:

$$v_{slip} = \frac{\tau}{\mu} h_w. \quad (15)$$

This velocity should be used as boundary condition to the fluid solution on the interface: however, in all of the present computations its value is low enough to neglect any slip effect.

Similarly, the model allows for re-meshing of the fluid domain, moving the fluid domain boundary at an  $h_w$  distance from the actual solid wall, in order to take into account the obstruction effect of the water layer. The re-meshing is obtained by translation of the fluid nodes in the z direction, thus preserving the correspondence between solid-fluid interface faces and nodes, without the need of sophisticated interpolation procedures. Each element of the 2D water layer grid, even in such case, provides the correct boundary condition transfer through the gap between the deformed fluid domain and the solid one created by re-meshing.

However, re-meshing option did not have any significant effect in the present computations, since the average film height, as will be shown in the results, is too small to become significant.

### 3.3 Droplet condensation

If the film appears in the form of a discrete collection of still droplets, the droplet geometry does affect the effective heat transfer. Under the assumption of droplet size much smaller than the grid elements, we can analyse the typical geometry shown in Fig.2. It is worth to underline that we do not follow the details of the droplet shape nor simulate the time dependent behaviour of the air-flow interface, but include in the model those aspects which may significantly affect the heat transfer latent flux, such as the different surface which take part to the condensing process (Fig.2). These are:  $A_{wet}$  is the area of the droplet/solid interface,  $A_{dry}$  is the area of the dry portion of the solid surface,  $A_{cap}$  is the area of the droplet/fluid interface, here assumed to be a spherical cap defined by the contact angle  $\theta$ , and  $A_t$  is the total area of the solid surface.

The heat balance in this case is:

$$Q_s'' = Q_{conv}'' \frac{A_{wet}}{A_t} + Q_{conv}'' \frac{A_{dry}}{A_t} + \dot{m}_c'' \frac{A_{cap}}{A_t} \lambda. \quad (16)$$

When condensation of water vapour takes place on a solid surface, nucleation of droplets occurs. The contact angle of the droplets during this phase can be assumed as the advancing contact angle. When droplets cover a large part of the surface coalescence or fusion will occur, but since coalescence preserves volume a release of free surface follows, allowing for new nucleation. This leads to self similarity in the droplet pattern, with a stabilization of the value of the surface coverage close to the one corresponding

to close packing of small droplets. Assuming such self similar droplets distribution on the interface, the area ratios in Eq.(16) are constant, regardless of the droplet diameter. Thus we will assume the same value during all the condensation process, including the starting limiting case of diameter approaching zero. Moreover, the contact angle  $\theta$  will be assumed constant and equal to the static one. The diameter  $d$  of the droplet will correspond to a closely packed distribution of droplets with a cell-averaged height computed from the mass balance and the geometrical configuration:

$$\rho_w \frac{\partial h_w}{\partial \vartheta} = - \frac{A_{wet}}{A_t} \dot{m}_c \quad (17)$$

$$d = \frac{12\sqrt{3}(\sin \theta)^3 h_w}{\pi(1 - \cos \theta)^2 (2 + \cos \theta)} \quad (18)$$

During evaporation, the behaviour of the droplet is more complex and has been commented in Croce et al. [5].

### 3.4 Transition from still droplet to moving film

Under external forces the drop changes in shape, becomes non spherical and is characterized by an hysteresis, imposed by the difference between the advancing  $\theta_{adv}$  and receding contact angles  $\theta_{rec}$ . The forces acting on the drop are: the drag force, driven by the external flow, the component of the gravitational force along the wall surface, and the rigidity force, which is the component of the surface tension along the moving axis, always opposite to the deformation direction. In the present computations, the gravitational force is much larger than the drag one, and so we can take advantage from the experimental results of ElSherbini [17]. According to ElSherbini [17], it is possible to

express  $\theta$  and  $\cos\theta$  along the droplet base contour as a polynomial function of the azimuthal angle  $\psi$ :

$$\theta(\psi) = 2 \frac{\theta_{adv} - \theta_{min}}{\pi^3} \psi^3 - 3 \frac{\theta_{adv} - \theta_{min}}{\pi^2} \psi^2 + \theta_{adv} \quad (19)$$

where  $\theta_{min}$  can be related to the Bond number:

$$\frac{\theta_{min}}{\theta_{adv}} = 0.01 Bo^2 - 0.0155 Bo + 0.97 \quad (20)$$

which represents the ratio of gravitational to surface tension forces:

$$Bo = \frac{\rho_w g d^2 \sin \alpha}{\sigma} \quad (21)$$

where  $g$  is the acceleration of gravity,  $d$  the drop diameter,  $\alpha$  the surface inclination angle and  $\sigma$  is the surface tension of the liquid air interface. Since gravity forces increases with  $d^3$ , shear stress forces with  $d^2$ , and surface tension forces only with  $d$ , a threshold value  $d_t$  exists such that we have still droplet for  $d < d_t$  and moving film for  $d > d_t$ . In our code, moving water is assumed in an element of the 2D interface grid if either the threshold diameter is exceeded or some runback water is flowing in from the neighbouring elements.

In narrow flow passages, the average water layer obstruction may become significant even before the drop-film transition: fluid domain re-meshing may help, in this case.

#### 4. Results and discussion

Different levels of detail in the water layer and mass transfer computation were tested in a range of different flow conditions. In particular, velocity effect is explored with four different inlet velocities, 0.3, 0.5, 0.75 and 1.5 m/s for an inlet relative humidity of  $\phi_0=0.5$ .

Furthermore, three different inlet relative humidity,  $\phi_0=0.5, 0.7, 0.9$  were tested at the same inlet speed of 0.5 m/s.

While in the film model the water height achieves the steady state, in the still droplet regime the water layer in the wet areas continuously builds up with time. The following computations were carried out for up to 20 seconds of physical time. In all of the considered cases, the water layer appears in the form of still droplet, as confirmed by Lin et al. Visualizations [1]. Although under such condition the water layer gets thicker and thicker, the area ratios in Eq.16 become constant, as soon as self similar droplet pattern is attained. If, as in our computation, the film turn out to be very thin and the water layer thermal resistance is negligible, these area ratios are the only condensate parameters influencing the heat transfer. Thus, also the heat transfer rate reaches a constant value as well. As a consequence, temperature distribution and dry area shape, which is related to the local dew temperature isoline, reach stable values. In the limit of very long time, however, the water layer will ultimately reach the threshold value and trigger the transition to either continuous film flow or moving droplets/rivulets. Thus, the results of the film model will also be presented, as it represents a possible asymptotic condition for long-term simulation, and in order to evaluate the discrepancies between the two approaches. It is worth notice, however, that still droplet configuration was reported by Korte and Jacobi [10] even after several hours of continuous operation.

Fig. 3 shows the fin temperature and the water layer average height distributions for the case  $\phi_0=0.5, v_0=0.75$  m/s. While the temperature fields look quite similar, the height distributions are significantly different. Furthermore, the extension of the dry area is slightly different. In the droplet model the active condensing area is only  $A_{cap}$ , rather than the whole available area  $A_{tot}$  (Fig.2). Thus, the condensing rate is smaller and the dry area

is larger. Experimental contour derived from Lin et al. shows that actually the droplet model is slightly more accurate. As stated above, the average water height distribution is quite different in the two cases: the moving film allows water drain in the streamwise direction, and on most of the fin surface it exhibits lower  $h_w$  with respect to the droplet model. Computation for the droplet model corresponds to a 10 second physical time, while the film model computation was stopped at convergence of the film height. However, the above defined transition criterion shows that at 10s the droplet are still quite far from the transition to continuum film, which might occur no earlier than after half an hour.

Furthermore, the water layer is quite thin, of the order of the micrometers (maximum value  $8,5 \mu\text{m}$  in Fig.3). Thus, thermal resistance effect are clearly negligible. For the droplet solution, since we are still in the steady droplet regime, also the gravity forces are not effective, while in the film model the streamlines gravity deviates water film streamlines towards the bottom of the fin. This leads to the characteristic shape of the higher film region (the red areas in Fig.3), which covers a smaller and smaller portion of the fin height  $H$  moving along the streamwise direction. Due to the small value of  $h_w$ , also water obstruction is, in the present computations, negligible.

The difference between heat and mass transfer analogy and full mass diffusion solution are highlighted in Fig.4. While temperature fields, again, show relatively small discrepancies, the average water layer film can be quite different. Fig.4 shows that the full computation allows for higher condensation, which is consistent with the small increase in fin temperature, and in the partially wet regime this leads to significant differences in the dry area shape and extension.

Different inlet velocities are compared in Fig.5 at the same inlet humidity of 50%. Differences are quite dramatic, and show that a little uncertainty in the experimental inlet

velocity value can easily mask, at least for the temperature field, the difference between different physical model of the water layer (Fig.3).

More quantitative comparison may be derived from the temperature profiles along the fin. In Fig.6 the temperature at  $x=25$  mm from droplet and film model are compared. We have actually a difference, which is small at low inlet humidity, and increase with  $\phi_b$ . Same considerations apply to the discrepancies between heat and mass transfer analogy and the full mass diffusion equation solution. As shown in Fig.7, again, we have differences which are a function of  $\phi_b$ : the two approaches give almost the same temperature at  $\phi_b=50\%$ , and have roughly up to 0.4 K difference at  $\phi_b=90\%$ . For most engineering applications, the heat and mass transport analogy would, thus, provide acceptably accurate temperatures in these simple geometries.

Finally, Lin et al. provide temperature profiles along vertical rows of thermocouples, as shown in Fig.1. In Fig.8, present results are compared with experimental data 25 mm downstream of the inlet section. Although the experimental data show a certain scattering, it appears that the complete mass transfer solution, together with the droplet water model, shows the best agreement with experiments.

#### 4. Conclusions

Different modelling approaches are considered for the analysis of thin condensing water layer along vertical fins. The results, compared with experimental data, show that the discrepancies between different approaches are not negligible. In particular, due to the non-uniform Dirichlet boundary condition in the mass diffusion equation, as well as the possibility of mixed Dirichlet-Neumann conditions for partially wet fins, the heat and mass transfer analogy does not completely reflects the physics of the problem. More

important, the actual structure of the water layer, which can be considered as a collection of still droplets, as confirmed by experimental evidence, rather than a continuous flowing film, has some impact on wall temperature, and a significant effect on both the evaluation of the actual water trapped between the fins, and the estimate of extension and shape of dry and wet regions. Thus, the combination of full diffusion equation solution should provide the most reliable predictions. Comparison with experimental data appears to support these considerations, although the uncertainty of literature measured values is quite high, in comparison with the magnitude of the differences between different models.

ACCEPTED MANUSCRIPT

**References**

- [1] Y.T. Lin, K.C. Hsu, Y.J. Chang, C.C. Wang, Performance of Rectangular Fin in Wet Conditions: Visualization and Wet Fin Efficiency, *ASME J. of Heat Transfer* 123 (2001) 827-836
- [2] C.C. Wang, Y.T. Lin, C.J. Lee, Heat and Momentum Transfer for Compact Louvered Fin-and-Tube Heat Exchanger in Wet Conditions, *Int. J. Heat and Mass Transfer*, 43 (2000), 3443-3452.
- [3] C.C. Wang, W.S. Lee, W.J. Sheu, Y.J. Chang, A Comparison of the Air Side Performances of the Fin-and-Tube Heat Exchangers in Wet Conditions: with and without hydrophilic coating, *Appl. Thermal Engineering*, 22 (2002) 2667-268.
- [4] G. Croce, H. Beaugendre, W.G. Habashi, Numerical simulation of heat transfer in mist flows, *Numerical Heat Transfer* 42 (2002) 139-152.
- [5] G. Croce, P. D'Agaro, F. Della Mora, Numerical simulation of glass fogging and defogging, *Int. J. Computational Fluid Dynamics* 19 (2005) 437-445.
- [6] C. Comini, G. Croce, Convective heat and mass transfer in tube-fin exchangers under dehumidifying conditions, *Numerical Heat Transfer, Part A* 40 (2001) 579-599.
- [7] C. Comini, C. Nonino, S. Savino, Numerical evaluation of fin performance under dehumidifying conditions, *J. Heat Transfer* 129 (2007) 1395-1402.
- [8] Y. Y. Yan, H. Lay, C. R. Gentle, J. M. Smith, Numerical analysis of fluid inside and around a liquid drop using an incorporation of multi-block iteration and moving mesh, *Chemical Engineering Research & Design*, 80 (2002) 325-331.
- [9] W. Shyy, H.S. Udaykumar, M.M. Rao, R. W. Smith, *Computational Fluid Dynamics*

- with Moving Boundaries, series in computational and physical processes in mechanics and thermal sciences, W. J. Minkowycz and E. M. Sparrow ed., 1996 Taylor&Francis, Washington.
- [10] C. Korte, A. M. Jacobi, Condensate Retention Effects on the Performance of Plain-Fin-and-Tube Heat Exchangers: Retention Data and Modeling, *ASME J. Heat Transfer* 123 (2001) 926–936.
- [11] A.I. ElSherbini, A.M. Jacobi, A Model for Condensate Retention on Plain-Fin Exchangers, *J. Heat Transfer* 128 (2006) 427–433.
- [12] X. Hu, L. Zhang, and A. M. Jacobi, Surface Irregularity Effects of Droplets and Retained Condensate on Local Heat Transfer to Finned Tubes in Cross-Flow, *ASHRAE Trans.* 118 (1994) 375–381.
- [13] D. Beysens, The formation of dew, *Atmospheric Research* 39 (1995) 215-237.
- [14] D. Beysens, Dew nucleation and growth, *Compte Rendues Physique* 7 (2006) 1082-1100.
- [15] J. Min, R.L. Webb, Condensate formation and drainage on typical fin materials, *Experimental Thermal and Fluid Science* 25 (2001), 101-111
- [16] C. Nonino, G. Comini, An equal-order velocity-pressure algorithm for incompressible thermal flows: Formulation, *Numerical Heat Transfer, Part B* 32 (1997), 1-15.
- [17] A.I. ElSherbini, A.M. Jacobi, Liquid drops on vertical and inclined surfaces II. A method for approximating drop shapes, *Journal of Colloid and Interface Science* 273 (2004) 566–575
- [18] Lepage, C. Y., Habashi, W. G., Conservative interpolation of aerodynamic loads for aeroelastic computations, *AIAA/ASME/ACSE/AHS/ Structures, Structural*

Dynamics and Materials Conference and Exhibit, 41st, Atlanta, GA; United States,  
3-6 Apr. 2000.

ACCEPTED MANUSCRIPT

**List of captions**

Fig.1 – Problem geometry.

Fig. 2 – Sketch of droplet geometry and parameters

Fig. 3 – Film and droplet model comparison,  $\phi_0=0.5$ ,  $v_0=0.75$  m/s. Left: temperature map. Right: color map of predicted average water layer height vs. experimental data (black line, [1])

Fig. 4 – Heat and mass transfer analogy (left column) and full mass transfer equation (right column) results comparison. Average water layer height,  $v_0=0.5$  m/s.

Fig. 5 – Air velocity effect.  $\phi_0=0.5$ . Interface temperature field

Fig. 6 –  $x/L=0.25$ , temperature profiles: comparison between film and droplet model

Fig. 7 –  $x/L=0.25$ , temperature profiles. Heat and mass transfer analogy and full diffusion equation solution

Fig. 8 – Fin temperature, 25 mm downstream of the inlet. Comparison with experiments [1].

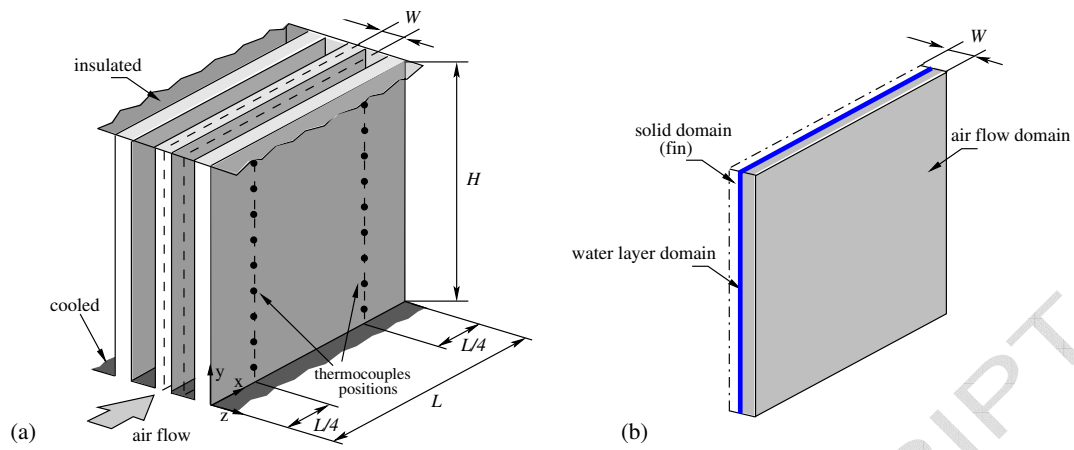
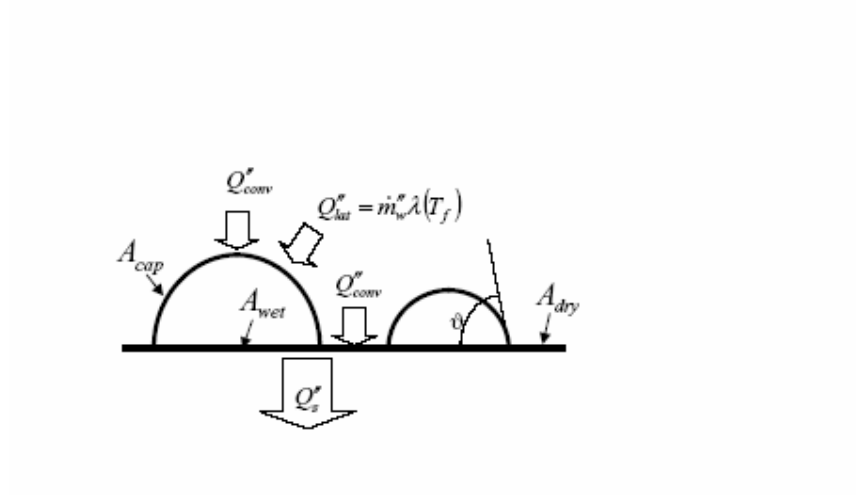


Figure 1

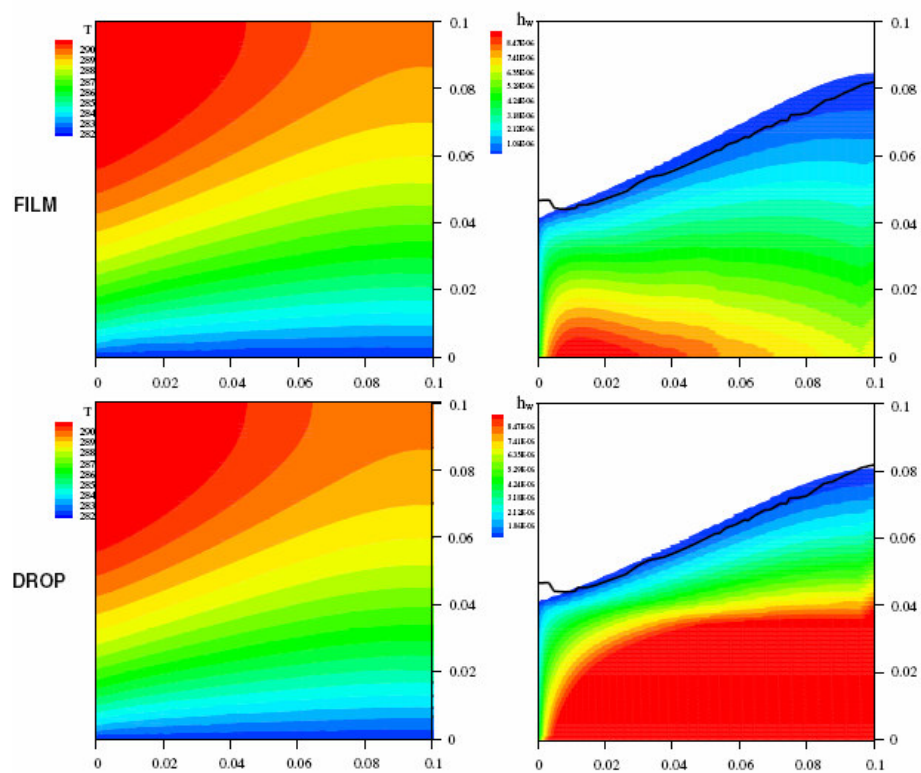
ACCEPTED MANUSCRIPT

Figure 2



ACCEPTED MANUSCRIPT

Figure 3



ACCEPTED

Figure 4

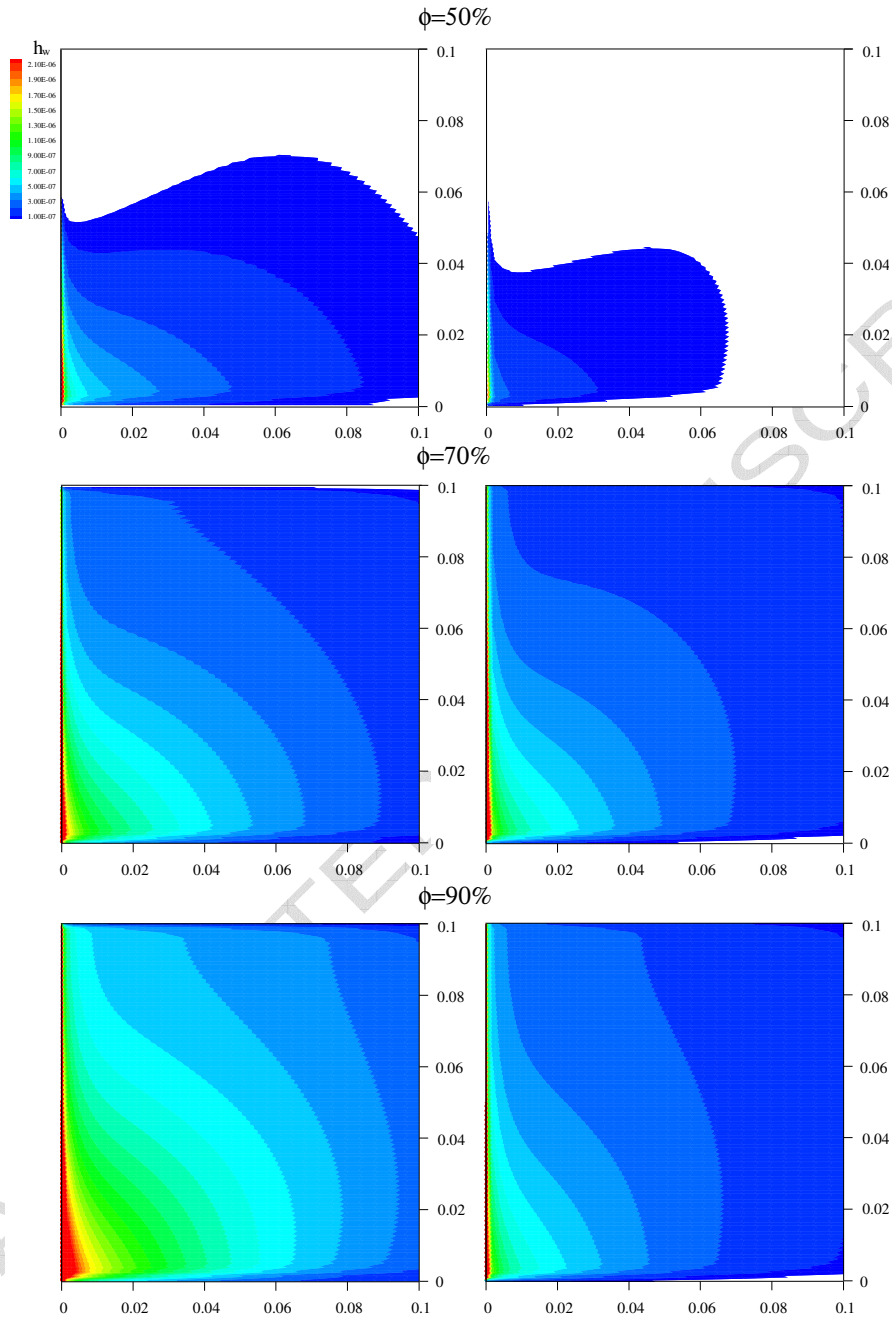
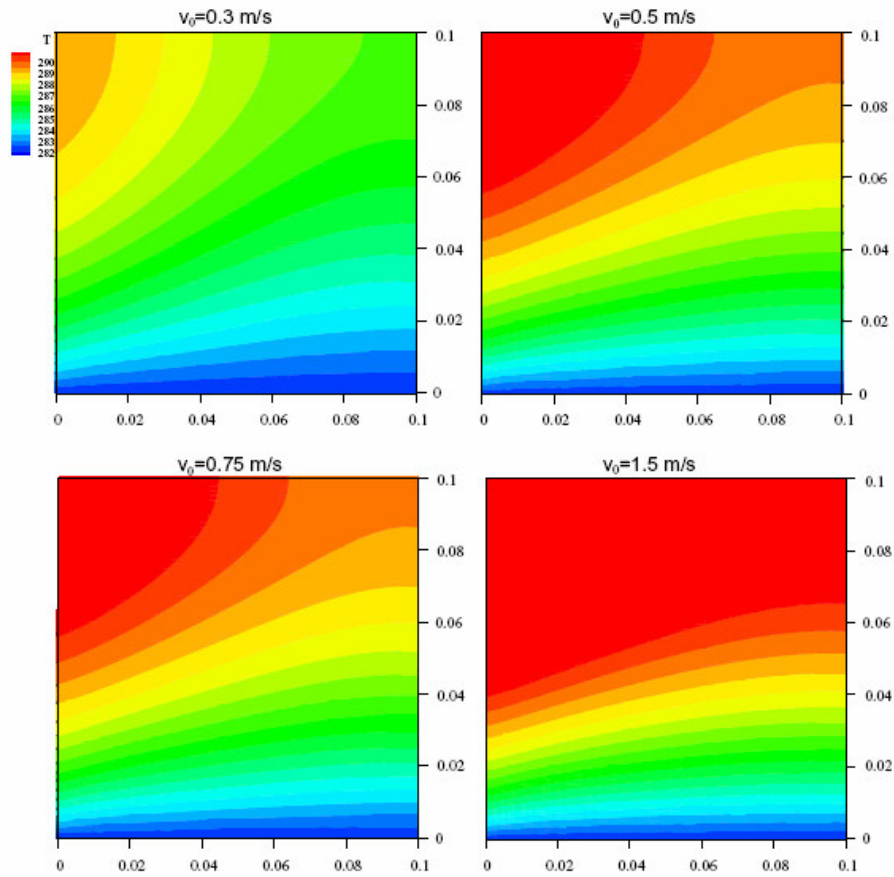
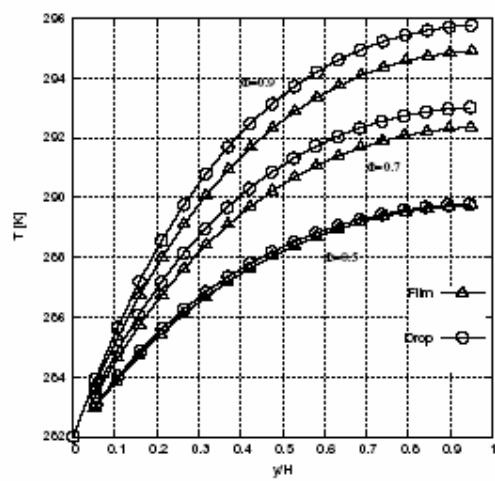


Figure 5



ACCEPTED

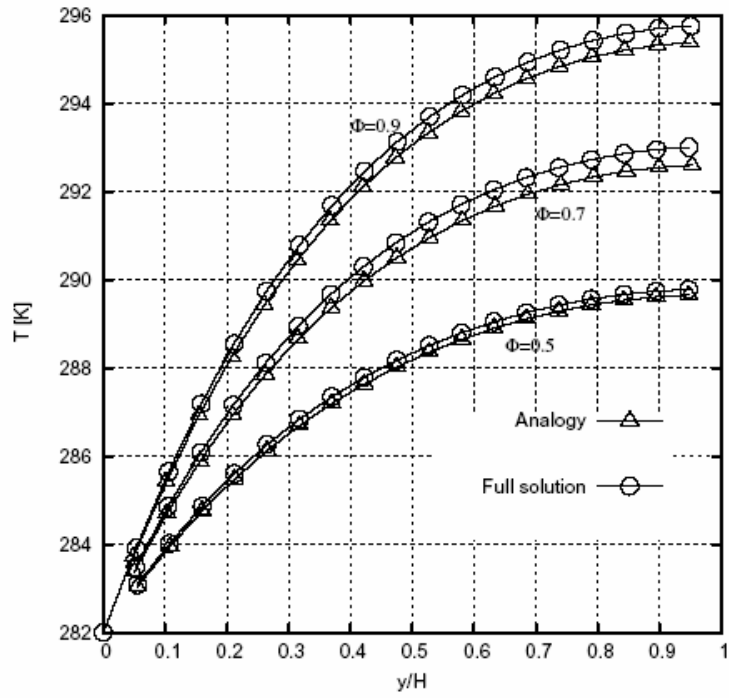
Figure 6



ACCEPTED MANUSCRIPT

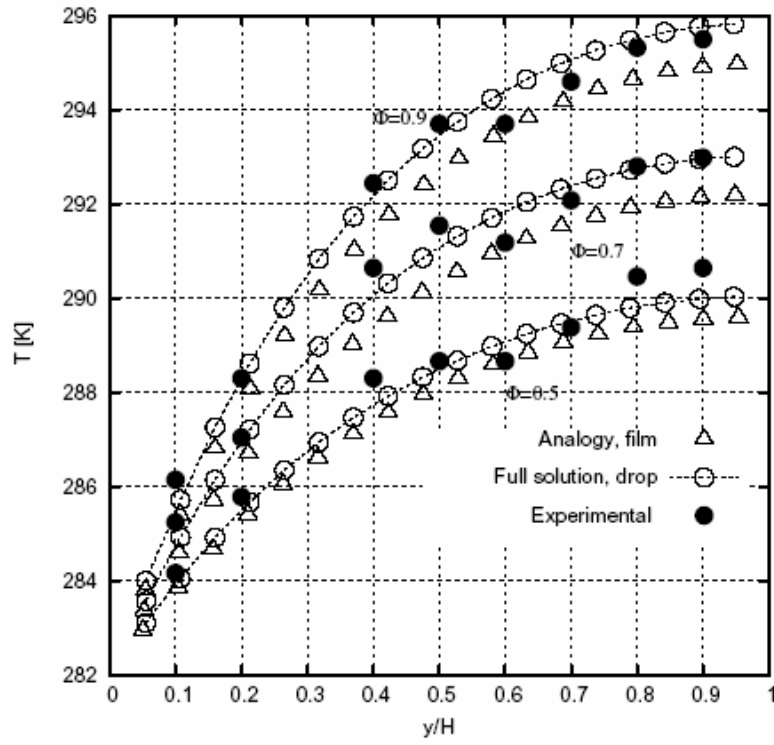
SCRIPT

Figure 7



ACCEPTED

Figure 8



ACCEPTED